Available online at www.sciencedirect.com
SCIENCE DIRECT®
ELSEVIER
Earth and Planetary Science Letters 217 (2004) 399–408
EPSL
www.elsevier.com/locate/epsl

The role of off-fault damage in the evolution of normal faults

Isabelle Manighetti [a,b,*], Geoffrey King [a], Charles G. Sammis [b]

[a] *Laboratoire de Tectonique, IPGP, 4, Place Jussieu, 75252 Paris Cedex 05, France*
[b] *Department of Earth Sciences, University of Southern California, Los Angeles, CA 90089-0740, USA*

Received 12 May 2003; received in revised form 9 October 2003; accepted 11 October 2003

Abstract

Recent measurements of slip profiles on normal faults have found that they are usually triangular in shape. This has been explained to be a consequence of on-fault processes such as slip-dependent friction. However, the recent observation that cumulative slip profiles on normal faults and fault systems in Afar are both triangular and self-similar excludes this explanation and requires some form of off-fault deformation. Here, we use elastic modelling to show that large triangular zones of off-fault damage can explain the observed triangular slip profiles provided damage is anisotropic in the form of cracks sub-parallel to the fault. Our modelling suggests that these triangular damage zones result from the enlargement of the crack tip damage area as the fault (or system) lengthens. Our modelling also demonstrates that different types of 'barriers' can cause the slip profiles to terminate abruptly at one or both fault ends, as observed in Afar and elsewhere.

Keywords: fault slip profiles; damage; Afar normal faults

1. Introduction

This article is a companion paper to Manighetti et al. [1] (hereafter referred to as Metal2001). Its objective is to explain slip distributions on normal faults. Simple theory suggests that they should be elliptical or bell-shaped (see discussion in Metal2001). However, accumulating data show such profiles to be rare. Triangular profiles are far more common (see [1,2] for a review). Metal2001 studied more than 300 active normal faults and fault systems in Afar with lengths varying from 0.1 to 60 km and ages from ~10 ka to 2 Ma. At most 15% of the corresponding profiles can be described as elliptical. The remaining have substantial linear portions and abrupt terminations, and show similar overall shapes regardless of scale, as illustrated in Fig. 1, where the slip profiles are grouped into the eight classes (a–h) adopted by Metal2001. Within each class, the profiles have been normalised to a common fault length and stacked to better show their characteristic shape. The shape typifying each class is inset in the upper left for each profile stack, and the percentage of faults that fall into each class is indicated (see discussion on shape classification in Metal2001). The most basic shape is that of a roughly symmetric triangle (Fig. 1a). All other shapes are shown to derive from this basic, trian-

* Corresponding author.
E-mail address: manig@usc.edu (I. Manighetti).

0012-821X/03/$ – see front matter © 2003 Elsevier B.V. All rights reserved.
doi:10.1016/S0012-821X(03)00601-0

gular shape (see discussion in Metal2001). The dominant slip profile shape is an asymmetric triangle (Fig. 1c). For the entire set also, the maximum slip (D_{max}) scales with fault length (L) as $D_{max} = 0.015L$, similar to values found in other studies (e.g. [2]). Since they have the same shapes, and displacement scales with fault length, the observed triangular slip profiles are self-similar.

The fact that the profiles do not have random shapes and are self-similar is of critical importance. King [3] has pointed out that self-similarity excludes traditional fracture models that assume fracture toughness to be a material property. Cowie and Scholz [4] then addressed this problem by tapering the ends of elliptical slip distributions using the Dugdale criterion. However, unlike the original concept, the taper lengths were not a material property but scaled with fault length. The form of their profiles, however, remained essentially elliptical. Other authors (see references in Metal2001) have suggested that varying fault friction or material inhomogeneity can explain deviations from an elliptical form. However, such processes should create random shapes and not the limited range of forms shown in Fig. 1. Moreover, slip-dependent friction invoked to explain individual triangular slip functions cannot explain self-similar forms (see discussion in Metal2001 and later in text). Linear slip functions can result where overlapping faults interact, but Metal2001 showed that they could not usually be explained in this way.

Metal2001 proposed qualitative models to explain these profiles. When a fault extends unimpeded, it develops the triangular slip profile shown in Fig. 1a. If a tip encounters a 'barrier', further lateral growth is inhibited and an abrupt drop in slip develops. Profiles b–f were explained in this way. Two profile stacks (g and h) are approximately elliptical or bell-shaped, but these are a small subset ($\sim$15%) of all profiles. The barrier hypothesis was supported by the observation that terminated slip profiles have a larger D_{max}/L ratio than triangular profiles, and by field observation of structures that might act as barriers.

While Metal2001 provided evidence that, in the absence of barriers, faults evolve with a triangular, self-similar slip profile, no clear mechanical process was proposed. They did, however, show that all previous explanations (references in Metal2001) fail to explain how a system of faults can develop a set of slip profiles that are both triangular and self-similar. In this paper, we propose a mechanical process capable of accounting for both these observations.

2. Developing a quantitative model of overall fault evolution

2.1. Modelling self-similar triangular slip profiles

The belief that cracks or faults should exhibit elliptical slip profiles is based on the analytic result that displacement across a stress-free or constant stress surface in an elastic medium develops an elliptical form (Fig. 2a) (e.g. [2]). Immediately beyond the fault tips the analytic result predicts infinite stress, which clearly cannot be sustained by real materials. Various suggestions have been offered to deal with this singularity that all effectively blunt the crack tip (see references in [2]). However, the resulting slip profile is bell-shaped, not triangular as observed. The result is that some additional processes are required to explain the triangular profiles.

The strain and stress distributions associated with a triangular slip function are shown in Fig. 2b for the simple case of Mode I crack. The stress along the fault plane is not constant, being higher towards the fault ends than at the centre. Hence, if a mechanism can be found to adjust the stress on a fault plane, then self-similar triangular slip functions may be explained. Furthermore, if the

→

Fig. 1. Rescaled and stacked cumulative slip distributions for Afar normal faults, as classified by Manighetti et al. [1]: (a) unrestricted, (b) tip-restricted, (c) half-restricted, (d) double tip-restricted 1, (e) double tip-restricted 2, (f) double tip-restricted 3, (g) elliptical with taper, (h) quasi-elliptical. Characteristic shape and percentage of faults belonging to each class is indicated in inset. About 12% of slip profiles could not be classified.

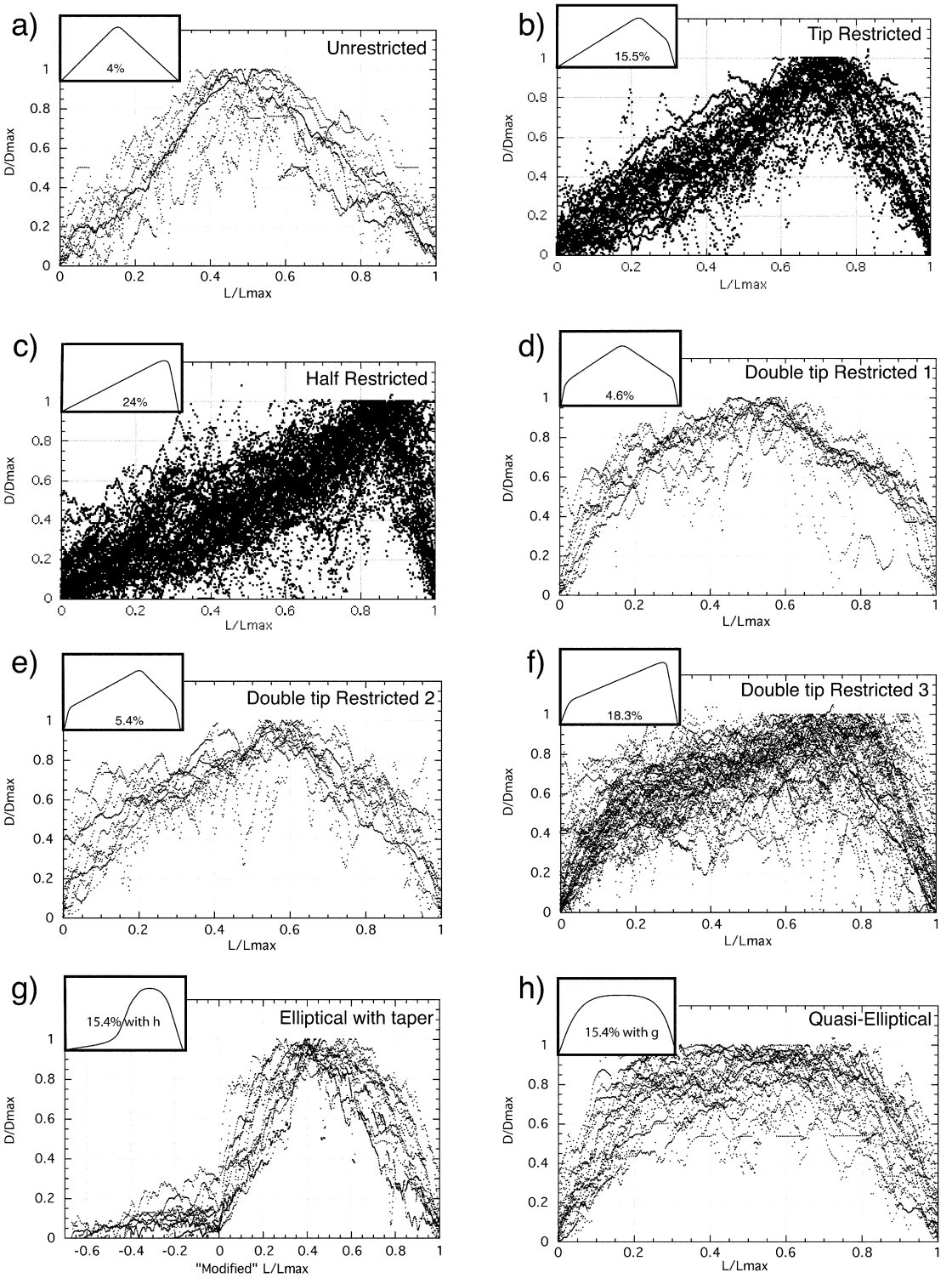
a)
Unrestricted
4%
b)
Tip Restricted
15.5%
c)
Half Restricted
24%
d)
Double tip Restricted 1
4.6%
e)
Double tip Restricted 2
5.4%
f)
Double tip Restricted 3
18.3%
g)
Elliptical with taper
15.4% with h
h)
Quasi-Elliptical
15.4% with g
D/Dmax
L/Lmax
"Modified" L/Lmax

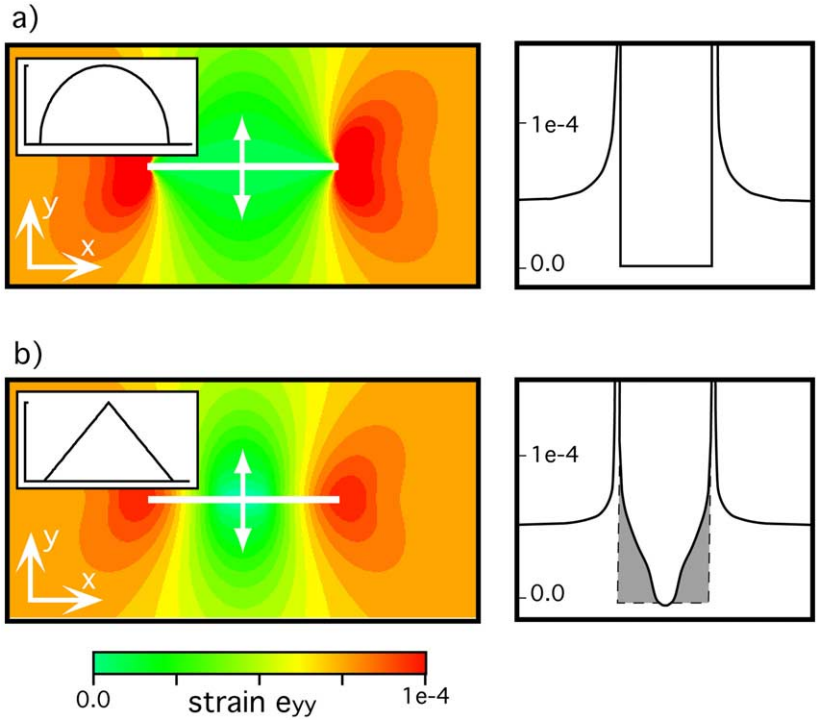

Fig. 2. Deformation associated with a dislocation having (a) an elliptical and (b) a triangular Mode I slip distribution. Panels on the left are strain distributions for the fault slip shown in inset. In each case the displacement to length ratio of the faults is 10^{-4}. A constant ε_{yy} strain of 5×10^{-5} is added to that resulting from the dislocations. Panels on the right show the ε_{yy} strain across the line of the dislocations. For the elliptical slip distribution in panel a the ε_{yy} strain and hence σ_{yy} stress across the dislocation is constant and taken to be zero. Stress at fault tips is infinite, while outside the dislocation ε_{yy} and σ_{yy} decay as $r^{-0.5}$ with distance r from fault tips. For the triangular slip distribution the ε_{yy} strain and hence σ_{yy} stress are lowest at fault centre and rise at fault ends. Outside the dislocation, ε_{yy} and σ_{yy} decay logarithmically with distance from fault tips. Stress across the dislocation in excess of that associated with an elliptical dislocation is indicated by shading.

stress on a fault plane can be arbitrarily adjusted, then any slip function can be created. Rock inhomogeneity and random variations of friction (or cohesion for Mode I cracks) could be and have been invoked to explain individual profiles (see references in Metal2001). However, only a limited range of slip profile types is observed regardless of scale (Fig. 1) so that an explanation invoking random processes seems improbable. A systematic process that could work for individual faults is to suppose that fault stress is related to fault displacement as a result of slip-dependent friction. If friction reduces as slip increases, then recently created and low slip parts of a fault would move less than an elliptical model would suggest. However, the self-similar (D_{max}/L = constant) profiles reported by Metal2001 cannot be explained in this way. Indeed, since long faults have slipped much more than short faults, the friction between their surfaces should be different so that self-similarity would not be preserved through the whole fault set. This statement can be generalised. Three self-similar triangular slip profiles and the stress distribution on the fault plane required to maintain them are shown in Fig. 3. Unlike slip, the stress profiles are self-affine in that the amplitude of the stress distribution does not scale with fault length (see [2] for a mechanical explanation). As a fault grows, the stress profile becomes stretched but its amplitude does not change. Since there is no simple way to generate a self-affine set from a self-similar set, there is no simple way to generate

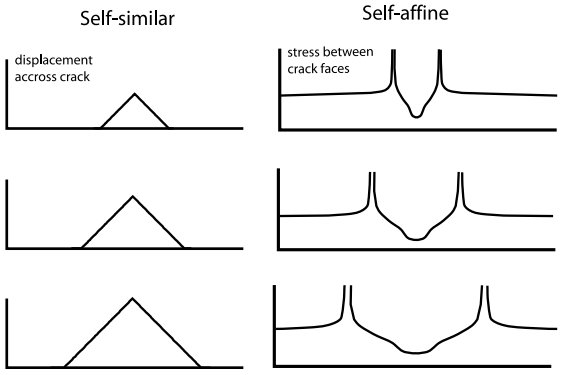

Fig. 3. Stress distributions for faults having self-similar triangular displacement profiles. The left column shows displacement for three faults whose maximum slip is proportional to length. The right column shows the associated strain or stress. For the displacement to be self-similar the stress amplitudes must remain the same but extend over a greater length. The strain–stress profiles therefore form a self-affine set.

the self-affine stress distribution from a friction profile that is a direct function of the self-similar slip profile. Hence, the observation of slip self-similarity is of major importance since it unequivocally demonstrates that the mechanical processes of fault evolution cannot be explained by on-fault processes alone.

An alternative to on-fault processes is suggested in Fig. 4. This shows an extensional fault, approximated by a Mode I dislocation, progressively extending and creating damage in the surrounding volume in the form of parallel tension cracks. As the fault lengthens, the zone in which cracks are created becomes larger, resulting in the formation of a damage zone with a triangular form.

The behaviour of such a system of cracks can be modelled using the boundary element methods of [5]. Fig. 5a shows the opening displacement of a major crack around which a series of parallel free opening smaller cracks have been introduced into the shaded triangular zones. The relative displacement between the major crack surfaces is plotted in Fig. 5b together with the elliptical profile that results without the smaller cracks. The opening is triangular in form. A series of tests was performed changing the crack density and the dimensions of the triangular damage zone. Provided there are sufficient cracks the results are similar. If the cracks are small, more are required; if they are larger, fewer are needed. The angle subtending at the centre of the fault by the triangular damage zone (β in Fig. 4a) can vary between 15 and 40° and an approximately triangular slip distribution is retained.

The presence of parallel cracks is important. If the shaded zones are modelled by regions of lowered modulus, the resulting slip profile is not triangular. Instead, deformation becomes greater than for an elliptical slip distribution near the

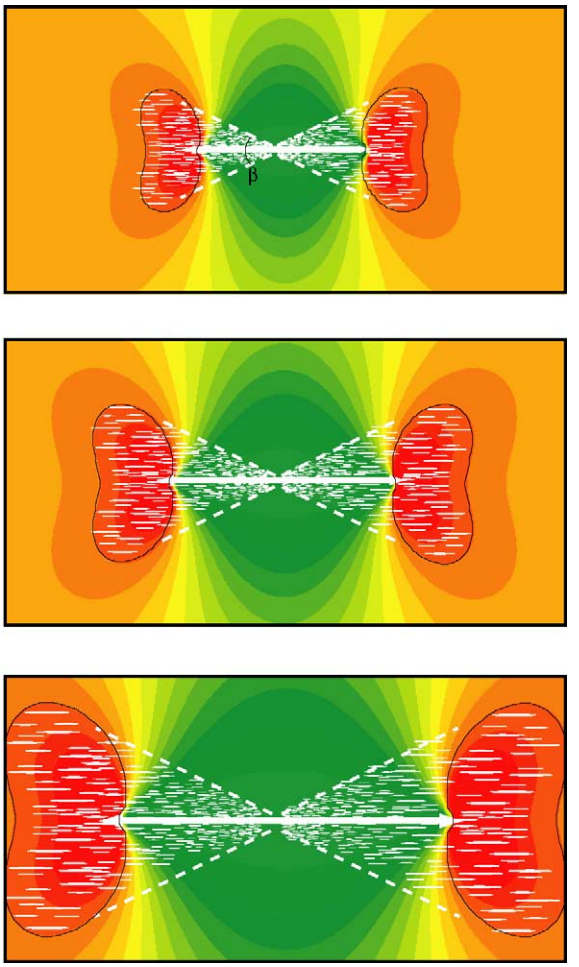

Fig. 4. Schematic evolution of damage associated with a fault lengthening in both directions from its centre. Colour scale is the same as in Fig. 2. When the strain reaches a threshold level, damage occurs as tension cracking. The area above the threshold enlarges as the fault length increases, producing a region of damage with a triangular form.

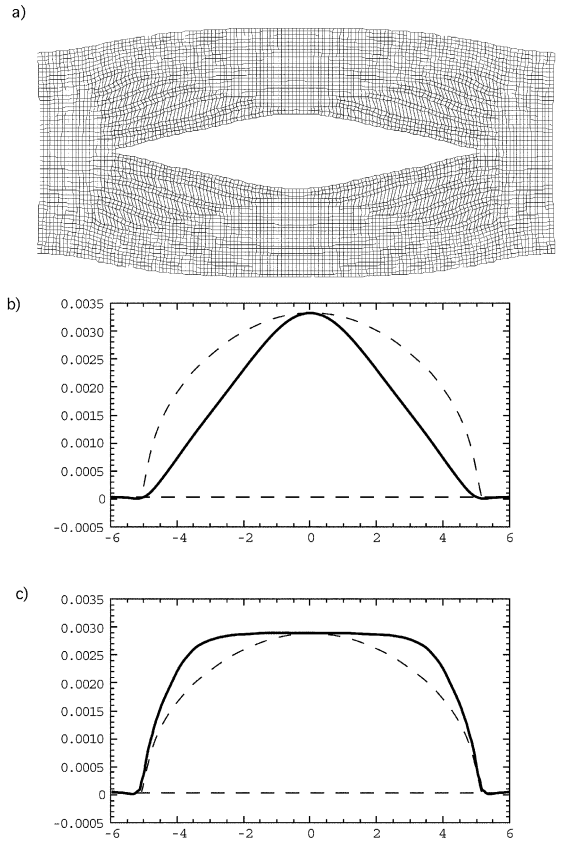

Fig. 5. Modelling triangular damage zones composed of freely opening cracks parallel to the main fault. Both fault and cracks are modelled by freely opening dislocations ($\varepsilon_{yy} = \sigma_{yy} = 0$). The system is driven by distant stress boundary conditions as in Fig. 2. (a) A grid for which deformation has been exaggerated by 5000 to permit deformation to be visualised. The form of opening is triangular. Parallel cracks are introduced in the four triangular shaded regions. (b) Opening displacement along the fault for the model shown in panel a. The slip profile is triangular. An elliptical slip distribution is also shown for comparison. (c) Slip distribution resulting from the model shown in panel a, modified so that the triangular shaded regions sustain a modulus reduction by a factor of 10 (no cracks are introduced). The slip profile is not triangular.

ends of the fault (Fig. 5c). The modelling consequently indicates that the triangular slip profiles result from anisotropic damage and cannot be explained by weakening alone.

In the Afar region studied by Metal2001, many tensile cracks or smaller faults parallel to major faults and systems are observed (e.g. [6,7]) and the mechanism described above may be sufficient to explain the observed slip profiles. However, both in Afar and elsewhere, identified damage and secondary faulting are commonly more pronounced on one side of a fault or a system of faults. Fig. 6 repeats the calculation of Fig. 5 but with damage restricted to one side of the fault. The resulting opening remains triangular in shape (Fig. 6b). In Fig. 6a it can be seen that the displacement on the undamaged side of the fault is closer to elliptical, but the triangular displacement on the damaged side is greater and dominates the total displacement.

Geological studies also note that secondary faults commonly fan out at the ends of major normal faults, systems, and extensional structures (e.g. [6–12]). In Fig. 7 we show that for modest angles ($< 10°$) these again result in triangular slip profiles.

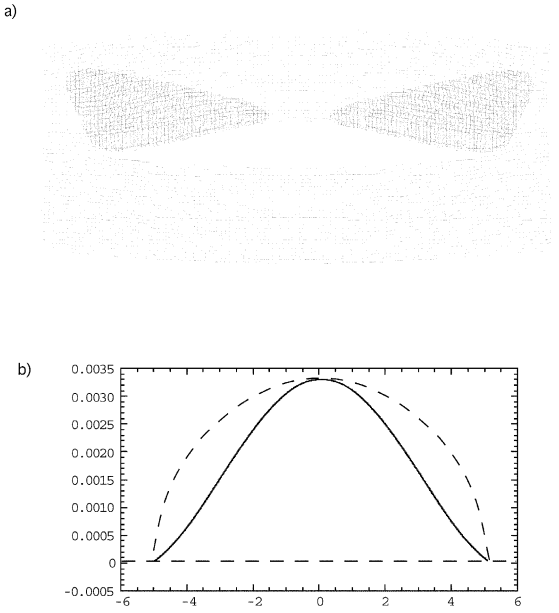

Fig. 6. Modelling triangular damage zones extending on one side of the fault only. In other respects, conditions are the same as for Fig. 5. (a) The grid is more deformed on the side of the fault subject to damage. The other side has a form more similar to an ellipse, but the amplitude is lower. (b) Opening displacement for the fault is dominated by deformation of the damaged wall and thus shows a triangular form.

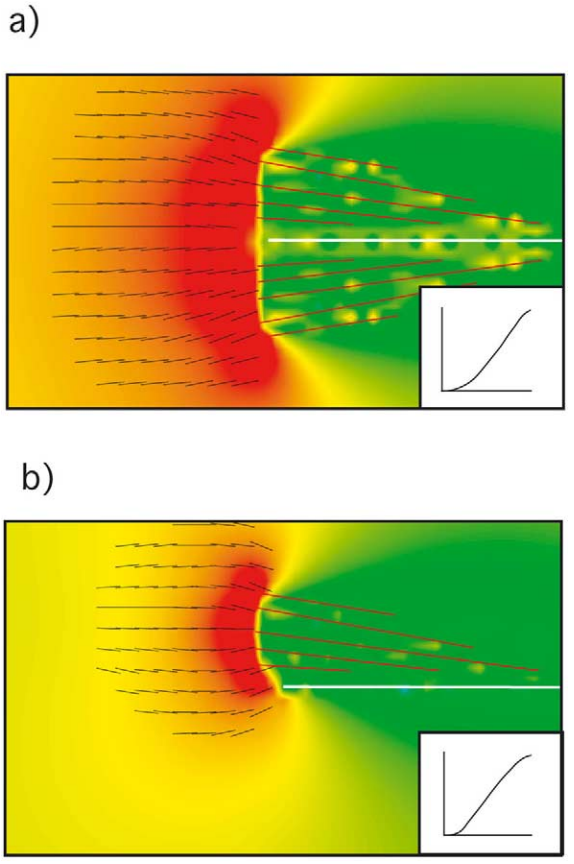

Fig. 7. Triangular damage zones composed of cracks at an angle to the main fault. Modelling conditions are, in other respects, the same as for Fig. 5 although only half of the fault is shown. Panels on the left show the strain–stress that tends to extend both the damage zone and the main fault. Small lines indicate the most favoured directions for new fracture. Inset panels show resulting displacement profile on the main fault. In panel a, damage extends on both sides of the fault. The resulting slip profile is triangular. In panel b, damage extends on one side of the fault. The resulting slip profile is also triangular.

The observed features in Afar include both fissuring and normal faulting, with the latter suggesting that the extensional features dip and are not perpendicular to the surface. The two-dimensional Mode I modelling that we adopt is consequently a simplification. However, it permits the known plate boundary conditions to be related to the observed features. While modelling with dipping features might create some surprises, it will prove difficult to implement and the main characteristics that we identify are likely to remain unmodified.

2.2. Modelling abrupt slip terminations

Metal2001 proposed that 'barriers' caused slip at the end of many faults and systems to terminate abruptly, and provide observational evidence in some cases. They suggest four such barriers, which we model in Fig. 8:

- A tough region that cannot be fractured easily (Fig. 8a).
- A low-modulus or multiply fractured region that distributes stress at the end of a propagating fault (Fig. 8b).
- A sub-parallel fault or major crack (Fig. 8c).
- A perpendicular fault or major crack (Fig. 8d).

Metal2001 noted that, with the exception of the case illustrated in Fig. 8a, such features are observed in the field.

2.3. Modelling slip irregularities within slip profiles

The cumulative slip profiles described by Metal2001 commonly exhibit irregularities that have comparable shapes to those observed for the whole fault. These authors proposed that a fault evolves by adding segments at its ends and that the slip distribution of the individual assimilated segments is preserved (or partly preserved) as the fault grows. Damage is therefore expected to occur at two scales: the scale of the segments, and the larger scale of the whole fault.

By using the numerical methods described earlier and by the principle of superposition, the slip distribution for an evolving system can be determined. Fig. 9a–c shows the evolution of a schematic fault through progressive addition of segments to give a 3-, 5- and 7-segment fault. The expected distribution of damage is shown as the fault evolves.

Fig. 10 shows a real slip profile and one possible interpretation of what the corresponding damage distribution could look like. At the largest scale, a triangular damage zone extends to become widest on the left of the figure. The abrupt termination of slip on the right is attributed to a barrier. In the example this is taken to be a region

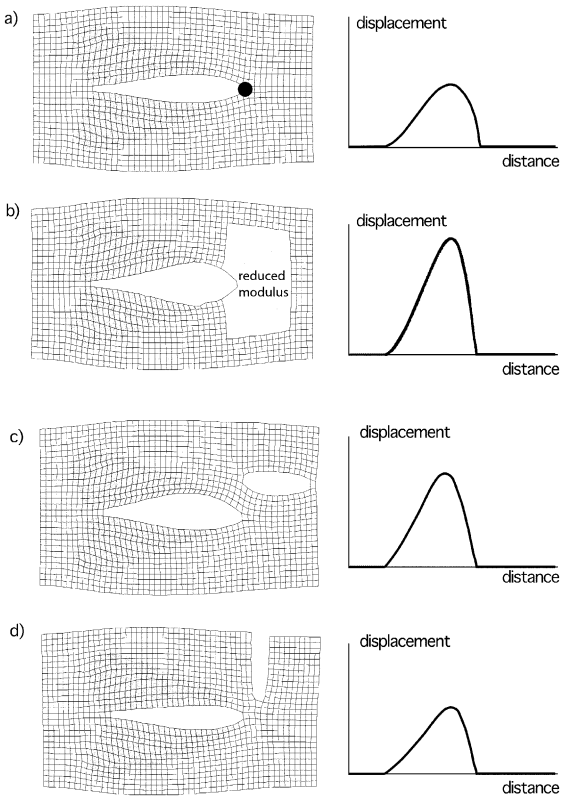

Fig. 8. Modelling abrupt terminations of slip at fault ends due to different barriers. Panels on the left show deformed grids, those on the right show the resulting slip profiles. Triangular damage zones are introduced on either side of faults as in Fig. 5, while different barriers are modelled at their right end. In each case the slip profile is an asymmetric triangle with maximum slip close to the barrier. In panel a, the barrier is modelled as a zone of high strength material. It results in arresting the propagation of the fault to the right, and is associated with high stress concentration at this fault end. In panel b, the barrier is modelled as a region of low modulus. It results in arresting the propagation of the fault to the right, but is not associated with high stress concentration. In panel c, the barrier is modelled as a secondary fault or fissure parallel to and offset from the main fault. In panel d, the barrier is modelled as a secondary fault or fissure perpendicular to and offset from the main fault.

where damage has resulted in the creation of fissures, both parallel and perpendicular to the main fault. This corresponds to a reduction of effective elastic modulus and hence a barrier of the type shown in Fig. 8b. At a smaller scale, triangular segment A is associated with (nearly) symmetrical damage similar to that modelled in Fig. 5. Segment B is asymmetric and a damage zone widening to the left is indicated to account for the linear section of the B profile. The abrupt reduction of slip on the right side of segment B is again attributed to a zone with lowered modulus similar to that which explains the abrupt slip termination of the main fault. The larger segment C is also associated with a triangular damage zone widening to the left, similar to that associated with segment B but larger in size.

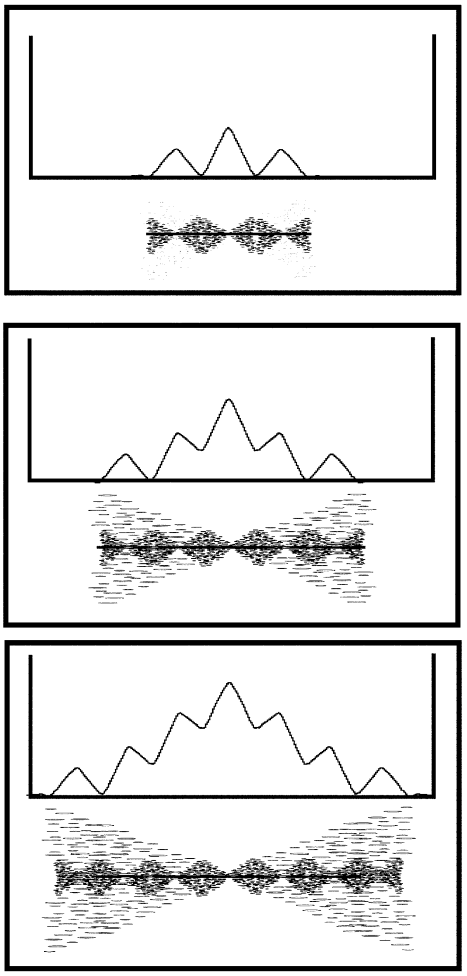

Fig. 9. Modelling a fault evolving through segment linkage. Calculations are performed as in Fig. 4 and the composite fault is created by repeated superposition of the linked segments. The damage distribution shown in each figure is schematic. The evolution of the fault involves damage at two different scales.

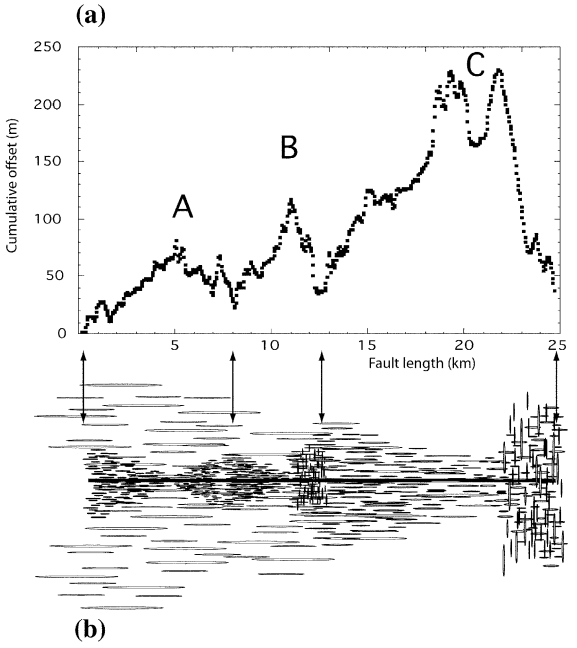

Fig. 10. The evolution of a real multi-segment normal fault. Panel a is an example of a multi-segment fault taken from Manighetti et al. [1]. The overall slip profile is half-restricted, as in Fig. 1c. At a more detailed level, the fault is made of three first-order smaller segments (A, B, C) now connected one to the other. A is rather tip-restricted in shape (as in Fig. 1b), while B and C are half-restricted (as in Fig. 1c). Panel b shows the schematic damage distribution consistent with both the overall shape and details of the slip distribution in panel a. At both the overall fault and segment scales, high slip gradients are taken to result from the existence of barriers, here supposed to be zones of multiple fracturing (similar to Fig. 8b). Linear sections of segment slip profiles are taken to result from development of small-scale triangular damage zones, while the linear section of the overall slip profile results from development of a triangular damage zone at a much larger scale.

The particular system above may involve different distributions of fissures from those shown schematically and the abrupt changes in slip may be due to other barrier effects. Nonetheless, until other possibilities are explored in the field, the proposed distribution is consistent with the fracture patterns observed in Afar. It can also be observed that in greater detail the profile consists of yet smaller triangular features that Metal2001 noted not to be the result of measurement error, which indicates that segments A, B and C have resulted from the assimilation of yet smaller segments.

3. Discussion and conclusions

The self-similar, triangular, cumulative slip profiles observed by Metal2001 cannot be explained by processes occurring on the fault planes or within the fault zones only. This excludes all of the mechanisms previously proposed to explain slip functions with linear trends, and in particular triangular slip functions (e.g. [13,14], and other references in Metal2001).

On the other hand, our modelling confirms the hypothesis of Metal2001 that, in the absence of features that form barriers, normal faults and systems can extend by developing approximately triangular slip profiles. The types of barriers hypothesised by the Metal2001 authors are confirmed by modelling to be capable of producing slip terminations as abrupt as those observed.

The simplest damage geometry that is consistent with the creation of triangular slip profiles consists of large triangular zones of damage with the apex centred on the assumed point of fault (or system) initiation. The damage must be anisotropic, as a uniform loss of strength by fracturing results in abrupt slip termination. Within this important limitation the parameters can be varied. The result is not very sensitive to the length and density of cracks, provided enough of them exist. Within the practical limits of modelling, the intuitive conclusion that many small fissures are as effective as a smaller number of larger ones appears to be supported. The angle with which the width of the zone increases is also not very critical as values between 15 and 40° seem to work. Triangular slip functions can also result if the fissures are at a modest angle to the main fault or system, as often observed in the field.

This study demonstrates that processes occurring on the fault plane (or within the fault zone) are not sufficient to explain the overall evolution of faults (or systems). Since most faults result from slip accumulated in numerous earthquakes, this suggests that on-fault processes are also in-

sufficient to explain the dynamics of earthquake ruptures, with wide-ranging implications for understanding earthquake processes.

The modelling has been restricted to Mode I crack opening approximating normal faulting. Although much harder to study, Metal2001 suggest that similar features can be observed for strike-slip faults. While the same requirement that off-fault deformation is important seems inevitable, we do not know if the same requirements of anisotropic damage must apply. A potentially important mechanical implication of this work is that a crack having a triangular slip profile is much more difficult to propagate than one having the traditional elliptical profile. Where the elliptical crack has an inverse square-root singularity at its tip and a stress intensity factor that scales with the square root of its length, a linear slip profile near the crack tip produces a logarithmic singularity and a stress intensity factor of zero. The only way that triangular cracks can propagate may be by linking with adjacent cracks, which may explain the ubiquitous observation of nested hierarchical slip functions as discussed earlier.

Acknowledgements

The authors thank David Bowman, A. Agnon and an anonymous reviewer for helpful reviews. This work has received support from INSU in France under programmes ACI Cat. Nat. and PNRN and the European Community's environment programme PRESAP. This is IPGP contribution No. 1954. The participation of CGS in this project has been supported by NSF Grant EAR-9902901 and by the Southern California Earthquake Center through cooperative agreement EAR-01016924 and the United States Geologic Survey cooperative agreement 02HQA60008.*[VC]*

References

[1] I. Manighetti, G. King, Y. Gaudemer, C. Scholz, C. Doubre, Slip accumulation and lateral propagation of active normal fault in Afar, J. Geophys. Res. 106 (2001) 13667–13696.

[2] C.H. Scholz, The Mechanics of Earthquakes and Faulting, 2nd edn., Cambridge University Press, 2003.

[3] G.C.P. King, The accommodation of strain in the upper lithosphere of the earth by self-similar fault systems; the geometrical origin of b-value, Pure Appl. Geophys. 121 (1983) 761–815.

[4] P.A. Cowie, C.H. Scholz, Physical explanation for the displacement-length relationship of faults using a post-yield fracture mechanics model, J. Struct. Geol. 14 (1992) 1133–1148.

[5] S.L. Crouch, A.M. Starfield, Boundary Element Methods in Solid Mechanics, Allen Unwin, Concord, MA, 1983.

[6] I. Manighetti, P. Tapponnier, P.Y. Gillot, V. Courtillot, E. Jacques, J.C. Ruegg, G. King, Propagation of rifting along the Arabia-Somalia plate boundary: Into Afar, J. Geophys. Res. 103 (1998) 4947–4974.

[7] I. Manighetti, P. Tapponnier, V. Courtillot, Y. Gallet, E. Jacques, P.Y. Gillot, Strain transfer between disconnected, propagating rifts in Afar, J. Geophys. Res. 106 (2001) 13613–13665.

[8] R. Weinberger, V. Lyakhovsky, G. Baer, A. Agnon, Damage zones around en echelon dike segments in porous sandstone, J. Geophys. Res. 105 (2000) 3115–3133.

[9] Z.K. Shipton, P.A. Cowie, Damage zone and slip-surface evolution over μm to km scales in high-porosity Navajo sandstone, Utah, J. Struct. Geol. 23 (2001) 1825–1844.

[10] D.C.P. Peacock, E.A. Parfitt, Active relay ramps and normal fault propagation on Kilauea volcano, Hawaii, J. Struct. Geol. 24 (2002) 729–742.

[11] L. Maerten, P. Gillespie, D. Pollard, Effects of local stress perturbation on secondary fault development, J. Struct. Geol. 24 (2002) 145–153.

[12] D. Marchal, M. Guiraud, T. Rives, Geometric and morphologic evolution of normal fault planes and traces from 2D to 4D data, J. Struct. Geol. 25 (2003) 135–158.

[13] P.A. Cowie, Z. Shipton, Fault tip displacement gradients and process zone dimensions, J. Struct. Geol. 20 (1998) 983–997.

[14] J.J. Walsh, A. Nicol, C. Childs, An alternative model for the growth of faults, J. Struct. Geol. 24 (2002) 1669–1675.